ENVIRONMENTAL ENGINEERING SCIENCE
Volume 41, Number 11, 2024

DOI: 10.1089/ees.2024.0076

Open camera or QR reader and scan code to access this article and other resources online.

Electrophoresis Characterization of Nanoplastic Particle Surface Charge in Dilute Aqueous Electrolytes

Jui-Yen Lin,[1,2,*] Ingyu Lee,[3] Cuijuan Feng,[2] Hyunook Kim,[3] and Chin-Pao Huang[2]

[1]*Department of Chemical and Materials Engineering, National Kaohsiung University of Science and Technology, Kaohsiung, Taiwan.*
[2]*Department of Civil and Environmental Engineering, University of Delaware, Newark, Delaware, USA.*
[3]*Department of Environmental Engineering, University of Seoul, Dongdaemun-gu, South Korea.*

Received: March 13, 2024 *Accepted in revised form: June 2, 2024*

Abstract

Aggregation, adsorption, and biofilm formation are involved in the fate and transport of nanoplastics in the aquatic environment. These interfacial processes are closely related to surface charge and electrical double layer (EDL) structure. As it is experimentally difficult to obtain surface potential, laser doppler electrophoresis is currently the most popular technique to measure zeta potential, or the potential at shear plane. However, the determination of zeta potential by laser doppler electrophoresis is not a trivial undertaking. Inaccurate zeta potential values could potentially lead to misleading conclusions. This study aims to present a comprehensive method tailored for nanoplastics to accurately measure zeta potential and convert it to surface charge and potential with classical EDL theory. The effect of particle size and number concentration on zeta potential measurement was investigated using monodisperse polystyrene (PS) latex. An optimal number concentration was between 10^{10} and 10^{12} #/L to generate sufficient scattered light with minimal interparticle interaction. Six nanoplastics were synthesized from major polymers to acquire the zeta potential at various pH, including low-density polyethylene, high-density polyethylene, polypropylene, PS, polyvinyl chloride, and polyethylene terephthalate. Based on classical EDL theory, the zeta potential measured at various ionic strength was converted to surface potential, revealing that the shear plane was 0.4 to 2.1 nm away from the surface. Finally, the surface charge density of nanoplastics was acquired, which is essential to describe interfacial processes of nanoplastics in the environment.

Keywords: electrical double layer; electrophoresis; microplastics; PS latex; scattering

Introduction

Extensive uses of plastics, because of low cost, high durability, and versatility, has created plastic pollution and severely threatened the aquatic ecosystem. The complexity of plastic products has hindered its recycling at a low 6–26% of recycle rate (Alimi et al., 2018). The accumulation of the plastic wastes in landfill and aquatic environment is projected to reach 33 billion tonnes by 2050. The environmental stresses, such as ultraviolet light, mechanical abrasion, and biodegradation, continue to fragmentate plastic wastes and generate secondary plastic particles. The plastic particles with diameter <5 mm are termed microplastics (MPs), whereas those having diameter <1 μm are often called nanoplastics (NPs) (Enfrin et al., 2019; Mitrano et al., 2021). Owing to high surface-to-volume ratio, NPs are susceptible to release plasticizers and adsorb toxins in the aquatic environment, raising human health concerns (Lehner et al., 2019). Although there is extensive information about the fate and transport of MPs (Yu et al., 2018), our understanding in NPs is lacking because of the difficulty in sampling NPs from the environment (Caputo et al., 2021; Fu et al., 2020).

Aggregation, coagulation, adsorption, and biofilm formation are involved in the fate and transport of NPs in aquatic environments (Lins et al., 2022). These interfacial processes are closely related to surface potential and charge density of NPs. For example, aggregation and coagulation of NPs depend on the total interparticle interaction energy, including attractive Van der Waals force and repulsive electrostatic force (Ali et al., 2023; Alimi et al., 2018; Kim et al., 2022). Accurate zeta potential and electrical double layer (EDL) profile are critical to estimate total interparticle interaction energy, a prerequisite to predict NPs' stability and critical coagulation concentration (Bayarkhuu and Byun, 2022; Li et al., 2019). Similar considerations are also

**Corresponding author:* Department of Chemical and Materials Engineering, National Kaohsiung University of Science and Technology, No. 415, Jiangong Rd., Samin Dist., Kaohsiung 80778, Taiwan; *E-mail:* jytlin@nkust.edu.tw

applicable for the attachment of NPs onto microorganisms in biofilm formation (Ganesan et al., 2022). The adsorption process concerns not only the surface potential but also the surface functional group. The adsorption of heavy metals onto hydrous solids, for instance, is controlled by the active sites capable of binding heavy metals via surface complexation reaction (Feng et al., 2023). These active sites can undergo protonation that results in surface charge density dependent of pH. Note that surface potential applying the theory of EDL readily estimates the surface active site density (Nguyen et al., 2022).

Among various electrokinetic techniques, laser doppler electrophoresis is currently the most popular method for zeta potential measurements (Thomas et al., 2017). In laser doppler electrophoresis, zeta potential is derived from electrophoretic mobility that is measured by light scattering of the moving particles in electric field. Multiple aspects of colloid science, such as light scattering, electrophoresis, and EDL structure, must be considered in zeta potential measurement. Several studies have reported precautions needed to acquire accurate zeta potential of nanoparticles (Bhattacharjee, 2016; Kobayashi, 2008; Lunardi et al., 2021; Nishiya et al., 2016; Tantra et al., 2010), which unfortunately had not been integrated in many studies on MPs and NPs. To ensure reliable electrophoretic mobility measurements, the quality of colloidal suspension is imperative. Earlier studies have indicated that the optimization of number concentration of particle is essential to prevent multiple scattering (Lunardi et al., 2021; Tantra et al., 2010). Moreover, the conversion of electrophoretic mobility to zeta potential is oversimplified by commercial instrument software, which typically provides only the following two models for limiting cases: the Hückel and Smoluchowski equations. However, the accurate conversion between these two limiting cases must be accomplished by the models that consider EDL relaxation (Kobayashi, 2008; Nishiya et al., 2016). Unfortunately, some research on NPs and MPs fail to provide sufficient information on samples or the equation used to convert electrophoretic mobility to zeta potential. In some cases, even the basic details such as solution pH, type of electrolyte, and ionic strength were absent, which are vital for the elucidation of surface charge density and potential (Behrens et al., 2000; Chassagne and Ibanez, 2014).

This study aims to present a comprehensive protocol specific for NPs to acquire accurate zeta potential using laser doppler electrophoresis. The principles of light scattering, electrophoresis, and EDL theory were briefly revisited. The effect of size and number concentration on zeta potential measurement was exemplified by polystyrene (PS) latex given their narrow size distribution and high stability in dilute electrolyte. Six types of NPs, synthesized from bulk polymers of low-density polyethylene (LDPE), high-density polyethylene (HDPE), polypropylene (PP), PS, polyvinyl chloride (PVC), and polyethylene terephthalate (PET), were used to acquire their zeta potential at various pH and electrolytes. Surface potential and surface charge density were derived from the zeta potential data with classical EDL theory, enabling the calculation of surface speciation with pH as the master variable.

Methods

Materials

PS latices with size of 50, 100, 300, 500, and 1000 nm were purchased from Polysciences Inc. (USA). The particle size of PS latex was measured by dynamic light scattering using Zetasizer (Nano-ZS, Malvern Panalytical, UK). The Z-average size was 52 ± 5 nm for 50 nm PS latex, 101 ± 2 nm for 100 nm PS latex, 311 ± 24 nm for 300 nm PS latex, 511 ± 7 nm for 500 nm PS latex, and 982 ± 150 nm for 1000 nm PS latex. The PS latex was considered to be monodisperse as the polydispersity index of all PS latices was <0.1. The number concentration of PS latex was estimated based on weight concentration provided by the manufacturer and density (Table 1).

Six NPs of the major polymers that account for 85% of plastics production, that is, LDPE, HDPE, PP, PS, PVC, and PET, were synthesized from bulk polymers to acquire their zeta potential at various ionic strengths and pH. The synthesis of NPs followed the homogeneous nucleation of dissolved polymer in appropriate solvent as reported in our previous work (Lin et al., 2023). Briefly, the bulk polymers were dissolved in their corresponding solvents—polyolefins in xylene, PS and PVC in tetrahydrofuran, and PET in trifluoroacetic acid. The solvent for nucleation was dimethyl sulfoxide for polyolefins and water for PS, PVC, and PET. After sequential filtration to remove aggregates and large particles, the synthesized NPs were obtained. The synthesized NPs were spheroids with a diameter between 100 and 1000 nm (Supplementary Data S1). Stock suspensions with number concentration around 10^{14} #/L were prepared by redispersing the synthesized NPs in 20 mL of 30 mg/L of Tween 20 (half of its CMC at 25°C). The stock suspensions were stored at 4°C.

Sodium perchlorate ($NaClO_4$), sodium nitrate ($NaNO_3$), and sodium chloride (NaCl) were purchased from Fisher Scientific (USA) and used as inert electrolytes. The deionized water with resistivity greater than 18.2 MΩ-cm was used to prepare all solutions.

Electrophoretic mobility measurement

The commercial PS latex with size of 50–1000 was used to investigate the effect of size and number concentration on electrophoretic mobility measurement given its sharp size distribution and stable zeta potential in neutral pH. The PS latex suspensions in 10^{-2} M $NaClO_4$ were prepared by sequential dilution to obtain a wide range of number concentration (10^7–10^{14} #/L). The pH of PS latex suspension was 8.7 ± 0.3. The electrophoretic mobility was measured within 1 day. An aliquot volume (1 mL) was transferred to the zeta meter cuvette (folded capillary zeta cell, DTS1070, Malvern Panalytical) using a Pasteur pipette. The electrophoretic mobility was

Table 1. Refractive Index and Density of Polymers Used in This Research

Polymer	*Density (kg/m^3)*	*Refractive index (–)*
LDPE	890–930	1.586
HDPE	940–990	1.540
PP	870–920	1.473
PS	1040–1070	1.592
PVC	1400–1420	1.539
PET	1370–1455	1.575

HDPE, high-density polyethylene; LDPE, low-density polyethylene; PET, polyethylene terephthalate; PP, polypropylene; PS, polystyrene; PVC, polyvinyl chloride.

represented by the average of five measurements with an error bar of standard deviation.

The synthesized NPs of six major polymers, including LDPE, HDPE, PP, PS, PVC, and PET, were used to study the effect of pH and ionic strength on zeta potential. Fifty-milliliter suspension of synthesized NPs with number concentration of 10^{11}–10^{12} #/L was prepared by diluting the stock suspensions with electrolyte. Note that the final concentration of Tween 20 in the samples was around 0.3 mg/L, equivalent to surface coverage of 0.2 mg/m^2 for NPs with d of 700 nm. As a nonionic surfactant, the effect of Tween 20 on zeta potential is from the shift of shear plane, which should be insignificant at such low surface coverage. The zeta potential measurement of the synthesized NPs was performed with a fast titration technique. Specific amounts of acid ($HClO_4$, HNO_3, and HCl) and NaOH were added to the suspension for pH adjustment. After 30 min, the pH of the suspension was measured, and 1-mL aliquot was withdrawn for electrophoretic mobility measurement. The process was repeated to cover a wide range of pH from 2 to 10. The ionic strength was corrected based on the amount of acid and base added.

Analytical method

The electrophoretic mobility (u_e) of the suspension was measured with Zetasizer (Nano-ZS, Malvern Panalytical) by the laser doppler electrophoresis method. He-Ne laser (633 nm, 4.0 mV) was the light source. Based on the scattering efficiency of the sample, the incident laser was attenuated automatically at a proper level before reaching the sample, creating the scattering light to be detected by an Avalanche photodiode at 90° to the incident laser. A direct current was applied to the cuvette, creating an electric field up to *c.a.* 20 V/cm for measurements. For charged particles, the electric field would induce electrophoresis, causing the scattered light to exhibit a frequency shift owing to doppler effect. The algorithm of phase analysis light scattering enables the analysis of the phase difference between the laser beam and scattered light, which is further converted to the terminal velocity of particles (v_t). With the assumption that the velocity is only brought by electrophoresis, the electrophoretic mobility (u_e) can be obtained according to Equation 1. For spherical particles whose frictional force obeys Stokes' law, the electrophoretic mobility can be expressed as Equation 2 (Supplementary Data S1, Supporting information).

$$u_e = \frac{v_t}{E} \tag{1}$$

$$u_e = \frac{2\varepsilon_0 \varepsilon_r \zeta}{3\eta} f(\kappa R_s, \zeta) \tag{2}$$

where u_e is the electrophoretic mobility of particles (m^2/V/s), and v_t is the terminal velocity of particles (m/s) in the applied electric field (E, V/m). ζ is the zeta potential (V), ε_0 is the vacuum permittivity (8.85×10^{-12} C/V/m), ε_r is the relative dielectric constant of water (78.5 at 25°C), and η is the absolute viscosity of water (0.001 kg/m/s at 20°C). The function $f(\kappa R_s, \zeta)$ is the correction for EDL and electric field distortion, to be discussed in detail.

Quality control

To ensure the accuracy and reliability of electrophoretic mobility measurement, precautions were taken to prevent the contamination of alien particulates. Deionized water and the prepared electrolyte solution were filtered through 0.22-μm cellulose acetate filter membrane (Fisher Scientific, USA). All containers were rinsed thoroughly with filtered deionized water. The preparation of the suspensions of PS latex and synthesized NPs was done in a laminar flow cabinet. The zeta potential measurement by Zetasizer was validated using zeta potential standards (ZTS1240, Malvern Panalytical) every week. According to the manufacturer's document, the least count rate is 20 kilo counts per second (kcps) for reliable measurements. The lowest number concentration of PS latex and synthesized NPs was estimated using the Concentration Utilities Calculator in Zetasizer Software (Malvern Panalytical). For PS latex of different sizes, the concentration to produce 20 kcps of scattered light was 2×10^{11}, 5×10^9, 6×10^6, 6×10^5, and 5×10^5 #/L for 50 nm, 100 nm, 300 nm, 500 nm, and 1000 nm PS latex, respectively. For synthesized NPs, the lowest concentration of detection was 3×10^5 #/L for LDPE, 1×10^6 for HDPE, 3×10^6 for PP, 1×10^8 for PS, 7×10^7 for PVC, and 2×10^7 for PET. The number concentration of all samples was greater than the lowest concentration shown previously. The measurement of electrophoretic mobility was conducted for 5 times with automatic adjustment on voltage, laser attenuation, and number of replicates.

Results and Discussion

Effect of particle size on electrophoretic mobility

The laser doppler electrophoresis technique measures the electrophoretic mobility by analyzing the phase shift of the scattered light from the particles moving in an electric field. In commercial instrument software, the terminal velocity of particles is assumed to be driven by electric field alone, that is, electrophoresis (Eq. 3). However, sedimentation could contribute to particle movement (Eq. 4). Figure 1 shows the velocity

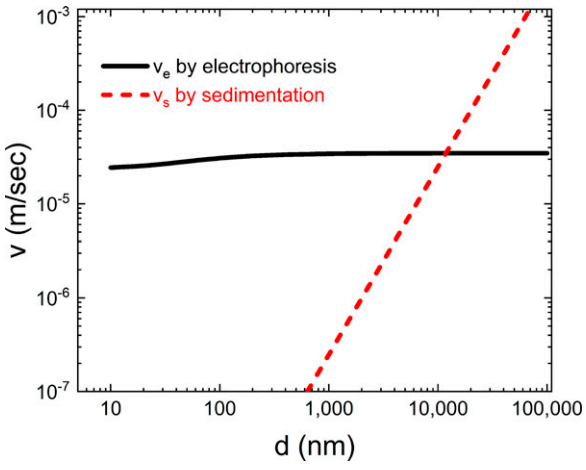

FIG. 1. Distribution of terminal velocity because of electrophoresis (v_e) and sedimentation (v_s) of plastic particles as a function of particle size. (Plastic = PET, ρ_s = 1384 kg/m^3, ζ = –25 mV, E = 20 V/cm, $I = 10^{-2}$ M, corrected by Ohshima's model).

as a function of particle size owing to sedimentation and electrophoresis under E of −20 V/cm, exemplified by PET. PET is one of the heaviest polymers in the present study with a density of 1370–1455 kg/m^3 and has a zeta potential of −25 mV at neutral pH and ionic strength of 10^{-2} M. The electrophoretic velocity remains relatively constant at $\sim 3 \times 10^{-5}$ m/s regardless of size. The terminal velocity is dominated by electrophoresis as long as the particle size is smaller than 10,000 nm at which sedimentation velocity takes over. The result implies that the formation of aggregates could interfere with electrophoretic measurements because of the presence of particle destabilization agents, such as favorable electrolytes and hydrodynamics conditions. In contrast, the Brownian motion could affect the accuracy of electrophoretic mobility measurement, particularly for small particles (Karmakar, 2019). The observed velocity in laser doppler electrophoresis is a combination of electrophoresis and random thermal motion. That is, the measured velocity could suffer from fluctuation if Brownian motion is significant. The average Brownian motion velocity could be represented by the root mean displacement in random walk statistics (Supplementary Data S1, Supporting information). Under E of 20 V/cm, the average Brownian motion is 77%, 20%, and 17% of electrophoretic velocity at 10 nm, 50 nm, and 100 nm particle size, respectively. In this case, the distribution of electrophoretic mobility will be broadened by Brownian motion, diminishing the measurement quality and resolution (Scarlett, 2002).

$$v_e = \frac{2\varepsilon_0 \varepsilon_r \zeta f(\kappa R_s, \zeta) E}{3\eta} \tag{3}$$

$$v_s = \frac{2R_s^2(\rho_s - \rho_l)g}{9\eta} \tag{4}$$

where v_e and v_s are velocities (m/s) due to electrophoresis and sedimentation, respectively. ε_0 is the vacuum permittivity (8.85×10^{-12} C/V/m), ε_r is the relative dielectric constant of water (78.5 at 25°C), ζ is the zeta potential (V), $f(\kappa R_s, \zeta)$ is the correction function, E is the electric field (V/m), η is the absolute viscosity of water (0.001 kg/m/s at 20°C), R_s is particle radius (m), and ρ_s and ρ_l are densities of solid and medium, individually. g is the gravitational constant (9.8 m/s^2).

The scattering intensity and pattern are closely related to particle size and the difference in refractive index between medium and solids. The refractive index of water, that is, the medium, is 1.33. Table 1 lists the refraction index of the plastic particles used in this study (Grigorescu et al., 2019; Jabeen et al., 2017). The scattering pattern depends on the particle size relative to the wavelength of incident light, typically 532 and 633 nm in laser doppler electrophoresis instruments. For NPs smaller than 60 nm ($d < \lambda/10$), the scattering pattern can be described by the Rayleigh scattering. The scattering mode shifts to Mie scattering when the particle size is comparable to or larger than the wavelength of the laser. The Mie theory was adopted to model the effective cross-section area of scattering (C_{scat}) as shown in Figure 2a (Mätzler, 2002, p. 2). Generally, the scattering cross-section increased markedly with particle size, following a sixth-power relationship at $d <$ 100 nm, as predicted by the Rayleigh scattering (Niskanen et al., 2019). In other words, the electrophoretic mobility measurement of NPs with smaller size can be hampered by its low scattering efficiency. Furthermore, the direction of scattered light is influenced by particle size as well. Figure 2b shows the direction of the scattering of PS particle with various sizes as predicted by Mie theory. The incident light enters at 180°; the scattering efficiency is normalized to the intensity of forward scattering at 0°. For PS NPs with $d <$ 100 nm, the scattering pattern is rather symmetrical. At $d >$ 300 nm (0.5λ), backscattering dominates. As the detection angle in laser doppler electrophoresis is at 90°, the proportion of scattered light available for detection decreases.

Conversion of electrophoretic mobility to zeta potential

The zeta potential is calculated from measured mobility by electrophoresis theory (Eq. 5) involving a correction function $f(\kappa R_s, \zeta)$. This correction function is necessary owning to (1) the deformation of electric field by particle and (2) relaxation of EDL during electrophoresis (Hunter, 1981). The Henry's equation (Eq. 6) corrects the deformation of electric field because of the presence of particle and take the additional potential in EDL into consideration. Therefore, Henry's equation is a function of κR_s, or R_s/κ^{-1} with κ^{-1} being the thickness of EDL (Eq. 7). As shown in Figure 3a, the correction factor depends on κR_s: $f(\kappa R_s, \zeta) = 1.0$ at $\kappa R_s < 0.1$ and 1.5 at $\kappa R_s > 1000$ with a smooth transition in between. This yields

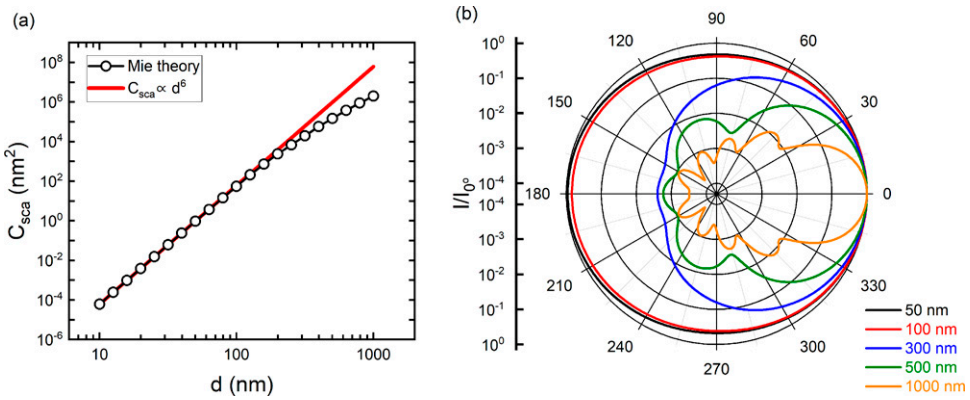

FIG. 2. **(a)** Relationship between cross-section of scattering (C_{sca}) and particle size of PS. **(b)** Polar diagram of scattering pattern of PS NPs of various particle sizes with incident light coming at 180° and intensity normalized to backscattering intensity at 0° ($I/I_{0°}$). (Medium = water, λ = 633 nm). NPs, nanoplastics; PS, polystyrene.

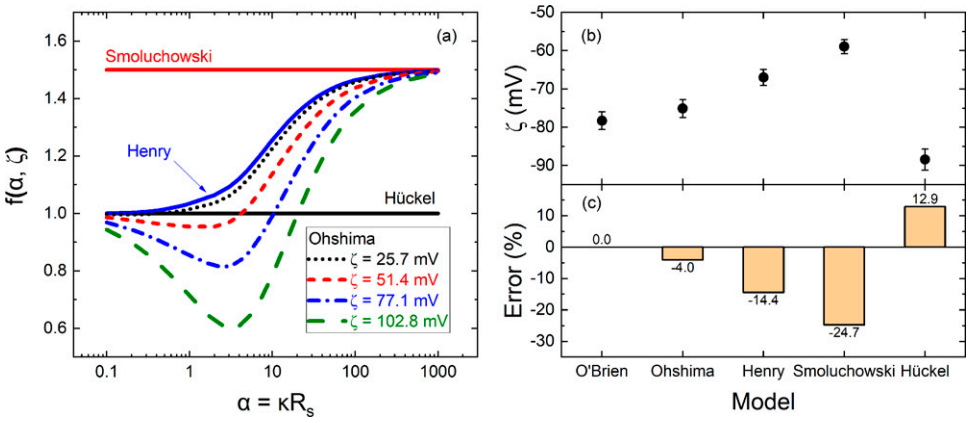

FIG. 3. **(a)** Values of correction function using Hückel equation ($f = 1.0$), Smoluchowski equation ($f = 1.5$), Henry's equation (Eq. 6), and Ohshima's model (Eq. 8). **(b)** Zeta potential estimated by various models and **(c)** error percentage compared with exact solution by O'Brien and White (100 nm PS latex, $I = 10^{-2}$ M $NaClO_4$, $\kappa R_s = 16.4$).

two limiting cases that are often used in the laser doppler electrophoresis software, that is, the Hückel equation at $f(\kappa R_s, \zeta) = 1.0$ and the Smoluchowski equation at $f(\kappa R_s, \zeta) = 1.5$.

The effect of EDL relaxation should be considered at high zeta potential value ($|\zeta| > 25.7$ mV). The EDL relaxation refers to the distortion of EDL during the migration of particles. As the charged particle and its ion atmosphere exhibit opposite charge, their direction of movement would be opposite in the electric field, thereby distorting the EDL from spherical into asymmetrical shape. O'Brien and White (O'Brien and White, 1978) have derived the governing differential equations that can only be solved numerically to obtain the exact solution (Supplementary Data S1, Supporting Information). Ohshima (Ohshima, 2001) provides an approximate form as shown in Equation 8, which is related to κR_s and the zeta potential of the particle. The value of the correction function was calculated using the Ohshima equation at zeta potential varying from 25.7 to 102.8 mV. As can be seen in Figure 3a, the effect of EDL relaxation is remarkable at intermediate κR_s and intensified as the zeta potential increases.

$$\zeta = \frac{3\eta u_e}{2\varepsilon_0 \varepsilon_r} \times \frac{1}{f(\kappa R_s, \zeta)} \tag{5}$$

$$f(\alpha) = \left(\begin{array}{l} 1 + \frac{1}{16}\alpha^2 - \frac{5}{48}\alpha^3 - \frac{1}{96}\alpha^4 - \frac{1}{96}\alpha^5 \\ - \left[\frac{1}{8}\alpha^4 - \frac{1}{96}\alpha^6\right] \exp(\alpha) \int_{\infty}^{\alpha} \frac{e^{-t}}{t} dt \end{array} \right)$$
$$\text{with } \alpha = \kappa R_s < 1 \tag{6a}$$

$$f(\alpha) = \left(\frac{3}{2} - \frac{9}{2}\alpha^{-1} + \frac{75}{2}\alpha^{-2} - 330\alpha^{-3} \right)$$
$$\text{with } \alpha = \kappa R_s > 1 \tag{6b}$$

$$\kappa^{-1} = \left(\frac{2F^2 I \times 10^3}{\varepsilon_0 \varepsilon_r RT} \right)^{-1/2} \tag{7}$$

$$f(\alpha, \zeta) = 1 + \frac{1}{2}\left[1 + \frac{2.5}{\alpha[1 + 2\ \exp(-\alpha)]}\right]^{-3} - \left(\frac{F\zeta}{RT}\right)^2 \left(\begin{array}{l} \frac{\alpha[\alpha + 1.3\ \exp(-0.18\alpha) + 2.5]}{2[\alpha + 1.2\ \exp(-7.4\alpha) + 4.8]^3} \\ + \frac{1}{2}\left(\frac{2\varepsilon_0 \varepsilon_r RT}{3\eta}\right)\left(\frac{1}{\lambda_+} + \frac{1}{\lambda_-}\right)\left\{\frac{9\alpha[\alpha + 5.2\ \exp(-3.9\alpha) + 5.6]}{8[\alpha - 1.55\ \exp(-0.32\alpha) + 6.02]^3}\right\} \end{array} \right) \tag{8}$$

where ζ is the zeta potential (V), u_e is the electrophoretic mobility (m^2/V/s), ε_0 is the vacuum permittivity (8.85×10^{-12} C/V/m), ε_r is the relative dielectric constant of water (78.5 at 25°C), $f(\kappa R_s, \zeta)$ is the correction function, E is the electric field (V/m), η is the absolute viscosity of water (0.001 kg/m/sec at 20°C), κ is the reciprocal thickness of EDL (m^{-1}), F is Faraday constant (96485 C/mol), I is ionic strength (M), R is ideal gas constant (8.314 J/mol/K), T is temperature (K), and λ_+ and λ_- are the drag coefficients of cation and anion, respectively. Equation 8 is generally applicable for $|\zeta| < 102.8$ mV at all κR_s values (Ohshima, 2001).

The use of adequate correction function is vital to acquire true zeta potential from measured electrophoretic mobility. For example, the electrophoretic mobility of 100 nm PS latex in 10^{-2} M $NaClO_4$ ($\kappa R_s = 16.4$) at neutral pH was -4.10 μm·cm/V·s. This mobility can be converted into five different zeta potentials depending on the correction function selected (Fig. 3b). The exact solution by O'Brien and White yielded the exact zeta potential of −78.3 mV. Ohshima model gave the closest correction function of 1.12 and a calculated zeta potential of −75.1 mV, which yielded the minimum error of 4.0%. As the Henry model did not consider EDL relaxation, the correction function was 1.32 and the calculated zeta potential was −66.9 mV, which was 14.4% smaller than the accurate value. In contrast, the Hückel equation overestimated the zeta potential by 12.9%, and the Smoluchowski equation underestimated the zeta potential by 24.7%. The result demonstrates that the conversion of electrophoretic mobility to zeta potential is not trivial. The use of limiting cases defaulted by commercial software could lead to significant discrepancy.

Effect of number concentration

To acquire a reliable electrophoretic mobility, the number concentration of particles should be optimized to produce sufficient scattering light but not too concentrated to cause interparticle interaction. The electrophoretic mobility of monodisperse PS latex with d of 50–1000 nm was recorded at a wide range of number concentration (10^7–10^{15} #/L) at pH 8.7 ± 0.3 in 10^{-2} M $NaClO_4$. The electrophoretic mobility was converted to zeta potential using the Ohshima's model (Eq. 8). Results shown in Figure 4a indicated that the number concentration of PS latex affected its zeta potential. The most negative electrophoretic mobility was observed at number concentration of 10^{11} #/L for all particle sizes. When the electrophoretic mobility of PS latex was normalized to that of 10^{11} #/L, a parabolic correlation between normalized mobility and log concentration appeared (Fig. 4b). Therefore, the optimal number concentration of submicron plastics for electrophoretic light scattering measurement was between 10^{10} and 10^{13} #/L, where the acquired mobility was deviated less than 10% from the most negative values. Although the number concentrations of PS latex were greater than the lowest concentration required for analysis, the quality of phase diagram could be compromised and affect determination of mobility. As the number concentration exceeds 10^{11} #/L, interparticle interactions occurred, which led to overlapping of EDL and particle aggregation (Hassan et al., 2015). Overcrowded particles could also result in multiple light scattering and attenuates scattered light intensity at the detector side (Bhattacharjee, 2016). Therefore, the electrophoretic mobility of the prepared plastic particles was measured at number concentration of 10^{10} and 10^{13} #/L to acquire accurate mobility and zeta potential.

Effect of pH and electrolyte

Figure 5 shows the effect of pH and ionic strength on zeta potential of NPs synthesized from six common plastics (LDPE, HDPE, PP, PS, PVC, and PET). All electrophoretic mobility measurements were conducted at the optimal number concentration of 10^{11}–10^{12} #/L. The zeta potential was calculated from electrophoretic mobility measurement following the Ohshima equation. Results clearly show that the zeta potential of these six plastic NPs was negative and varied with pH, exhibiting two plateaus at pH 4 and 10. The double sigmoidal zeta potential profile was due to the heterogeneous surface chemical structure. Lin et al. have reported that the surface of these synthesized NPs consists of nonpolar alkyl and polar oxygen-containing functional groups (Lin et al., 2023). The polar components could develop negative surface charge at high proton activity (~pH 3) through deprotonation of hydrated water molecules. The negative charge of nonpolar components relies on the specific adsorption of hydroxide ion at pH around 6. The pH-dependent zeta potential of NPs enables the evaluation of the surface acidity of plastic NPs (Lin et al., 2023).

It must be mentioned that the electrolyte and ionic strength of electrophoretic mobility (or zeta potential) measurements must be specified. Generally, zeta potential is measured in inert electrolyte to evaluate the intrinsic surface chemistry of particles in aqueous solution. Sodium perchlorate ($NaClO_4$) is considered the most inert electrolyte. Other inert salts include $NaNO_3$ and NaCl. Figure 5 shows that the zeta potential of all six synthesized NPs was nearly identical regardless of the background electrolyte, namely, $NaClO_4$, $NaNO_3$, or NaCl. This implies that ClO_4^-, NO_3^-, and Cl^- were not specifically adsorbed on surface, and the zeta potential resulted from the surface charge of intrinsic NPs' surface. In contrast, divalent cations such as those of alkaline earth members and divalent anion, specifically, sulfate, should never be considered because of possible specific adsorption onto the NPs' surface. Moreover, multivalent ions could neutralize surface charge and screen EDL more effectively than monovalent ions, causing a smaller absolute value of zeta potential (Kobayashi, 2008). Lu et al. (Lu et al., 2022) have studied the zeta potential of PS NPs in $NaNO_3$ and $Ca(NO_3)_2$ at the ionic strength of 10 mM and pH 8 and reported that the zeta potential in $Ca(NO_3)_2$ was −25 mV, which was 30% smaller than that in $NaNO_3$ (−38 mV). In conclusion, ionic strength and type of electrolyte should be always specified when reporting the zeta potential of NPs in aqueous solutions.

Surface potential and charge density

The surface potential of the hydrous solids cannot be measured experimentally in aqueous solutions. Fortunately, surface

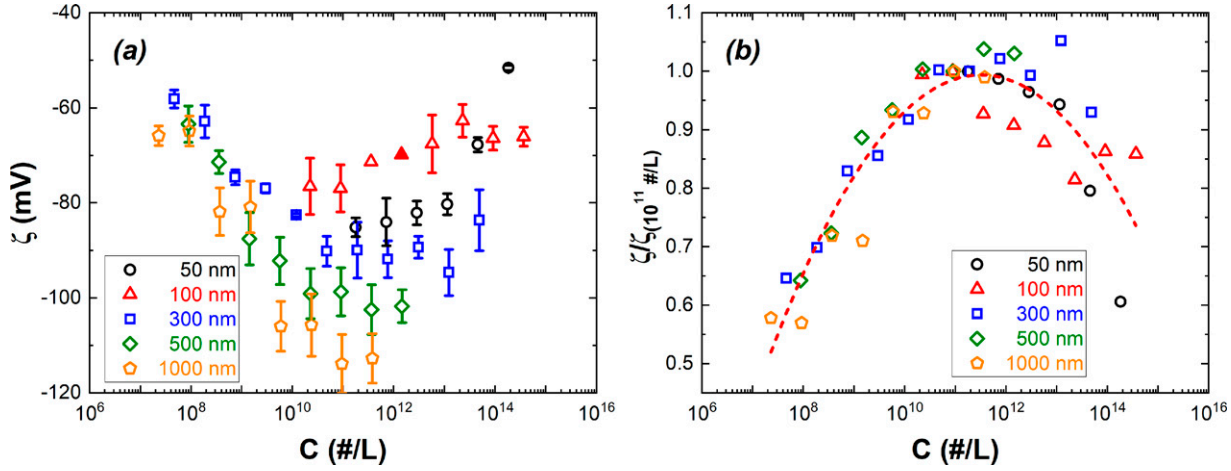

FIG. 4. **(a)** Zeta potential of PS latex as a function of number concentration. **(b)** Zeta potential normalized over particle concentration at 10^{11} #/L ($\zeta_{10^{11}/L}$) as a function of number concentration. *Red dashed line* was fitted by parabolic equation. ($I = 10^{-2}$ M $NaClO_4$, pH 8.7 ± 0.3, corrected by Ohshima's model).

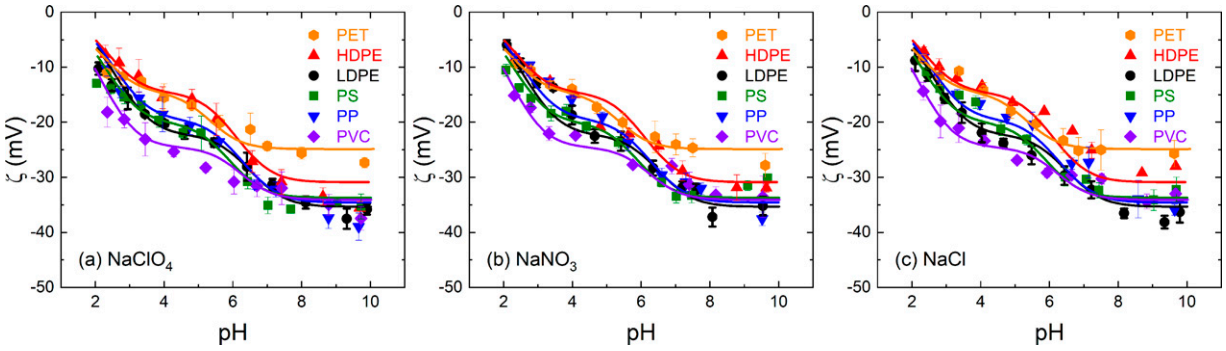

FIG. 5. Zeta potential as a function of pH for six resynthesized NPs at ionic strength of 3×10^{-3} M in **(a)** $NaClO_4$, **(b)** $NaNO_3$, and **(c)** NaCl. Lines represent average value of three measurements. (Number concentration = 10^{11}–10^{12} #/L, correction with Ohshima's model).

potential and the location of shear plane (at which zeta potential exists) could be determined with zeta potential measurements in various ionic strengths. Figure 6a shows the potential profile of hydrous solids with the following conditions: (1) constant surface potential (ψ_0), (2) rigid NP surface, and (3) surface potential follows the Gouy–Chapman EDL theory (Eq. 9) (Weng et al., 2001). Figure 6a shows that the potential drops as a function of distance from the surface and varies with ionic strength. The EDL is compressed as the ionic strength increases, leading to a decrease of κ^{-1} from 9.64 nm at $I = 10^{-3}$ M to 0.96 nm at $I = 10^{-3}$ M. Likewise, the zeta potential is predicted to be less negative from −44.4 mV at $I = 10^{-3}$ M to −16.7 mV at $I = 10^{-1}$ M if the shear plane was located 1 nm away from the surface.

As $\psi = \zeta$ at $x = d$, the Gouy–Chapman equation can be linearized with respect to the square root of ionic strength (Eq. 9c). Rearrangement of Equation 9c yields the explicit surface potential equation (Eq. 9d). Consequently, the position of shear plane (d) and surface potential (ψ_0) can be calculated from the slope and intercept of the linear $\ln[tanh9.74|\zeta|])]$ versus $\sqrt{I}$ plot, respectively, using the zeta potential obtained at pH 9 at $I = 10^{-3}$, 3×10^{-3}, and 10^{-2} M (Fig. 6b). Table 2 summarizes the estimated d and ψ_0 of the six freshly synthesized plastic particles. The high R^2 value suggests that the Gouy–Chapman EDL theory describes the EDL structure of these six NPs well. The position of shear plane was therefore estimated, varying from 0.4 to 2.1 nm. This range was comparable with amidine latex between 0.25 and 1.0 nm (Borkovec et al., 2000) and montmorillonite from 0.2 to 0.8 nm (Pei and Zhang, 2021). Kobayashi (2020) reported that a slip length at the interface of PS particle could be 1–3 nm, resulting in a faraway position of the shear plane (Kobayashi, 2020). Once the shear plane distance (d) is known, the surface potential (ψ_0) can be easily calculated from the zeta potential according to Equation 9d. Figure 7a gives the surface potential of the six synthesized NPs in 3×10^{-3} M $NaClO_4$, $NaNO_3$, and NaCl electrolytes (Fig. 5). Although the information of the surface potential and EDL structure is useful in predicting the stability of NPs, the study of many interfacial reactions necessitates the surface charge density (σ_0, C/m^2). The surface charge is calculated from surface potential based on the simple EDL theory (Eq. 10). Figure 7b shows the resulting surface charge density of six synthesized NPs in simple electrolyte at ionic strength of 3×10^{-3} M.

$$\tanh\left(\frac{F\psi}{4RT}\right) = \tanh\left(\frac{F\psi_0}{4RT}\right) \cdot \exp\left(-\frac{x}{\kappa^{-1}}\right)$$

for 1:1 electrolyte (9a)

$$\tanh(9.74\psi) = \tanh(9.74\psi_0) \cdot \exp\left(-\frac{x}{\kappa^{-1}}\right)$$

for 1:1 electrolyte at 25°C (9b)

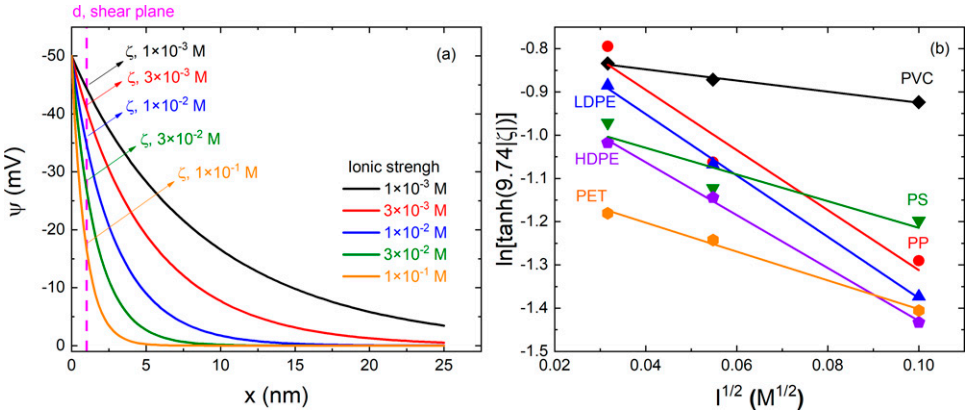

FIG. 6. **(a)** Surface potential profile of hydrous particles according to Gouy–Chapman electrical double layer theory at constant surface potential. **(b)** Plot of linearized Gouy–Chapman equation (Eq. 9c) for the determination of shear plane and surface potential based on zeta potential measured in 10^{-3}, 3×10^{-3}, and 10^{-2} M of $NaClO_4$ at pH 9.

Table 2. Summary of Shear Plane (d) and Surface Potential (ψ_0) Acquired from Linearized Gouy–Chapman Equation

NPs	*d (nm)*	ψ_0 *(mV)*	R^2
LDPE	2.1	−52.0	0.9980
HDPE	1.9	−48.7	0.9973
PP	2.1	−61.9	0.8948
PS	1.1	−46.3	0.7619
PVC	0.4	−49.9	0.9846
PET	1.0	−33.2	0.9895

This has been based on Figure 6b.

$$\ln[\tanh(9.74\zeta)] = (-3.28\times10^{9}d)\sqrt{I} + \ln[\tanh(9.74\psi_0)] \quad (9c)$$

$$\psi_0 = \frac{\tanh^{-1}\left[\tanh(9.74\zeta)\cdot\exp\left(\frac{d}{\kappa^{-1}}\right)\right]}{9.74}$$

for 1:1 electrolyte at 25°C (9d)

$$\sigma_0 = \sqrt{8\varepsilon_0\varepsilon_r k_B T n_\infty}\cdot\sinh\left(\frac{ze\psi_0}{2k_BT}\right) \quad (10a)$$

$$\sigma_0 = 0.1174\sqrt{I}\cdot\sinh(19.47\psi_0)$$

for 1:1 electrolyte at 25°C (10b)

where ψ_0 is the surface potential (V), x is the distance away from surface (m) at which the potential is ψ (V), d is the location of shear plane (m) at which the potential is ζ (V), κ^{-1} is the thickness of EDL (m), F is Faraday constant (96485 C/mol), R is ideal gas constant (J/mol/K), T is temperature (K), and I is ionic strength (M). σ_0 is surface charge density (C/m^2), ε_0 is vacuum permittivity (8.85×10^{-12} C/V/m), ε_r is the relative dielectric constant of water (78.5 at 25°C), k_B is Boltzmann constant (1.38×10^{-23} m^2-kg/s^2/K), n_∞ is concentration of electrolyte (m^{-3}), z is the valance of electrolyte, and e is electron charge (1.6×10^{-19} C).

The surface potential and surface charge density are pivotal to the fate of NPs in the environment. First, the relationship between surface charge density and pH can be used to describe the tendency of the protonation and deprotonation of surface, which is the foundation of surface acidity. In our previous study (Lin et al., 2023), the surface charge density of the six synthesized NPs was used to quantify their surface acidity. It was concluded that the surface acidity depends on the surface composition and heterogeneity because of aging. Once the surface acidity constants (K_a^{int}) and total sites ($\{S\}_T$) are known, we can predict the distribution of surface group as a function pH and thus the resulting surface charge. Second, in the study of heavy metal adsorption, it is essential to know both surface potential and surface charge density in order to calculate the stability constants of surface complexes as a means to model ion adsorption (Fan et al., 2019; Feng et al., 2023). Evaluation of the stability constant of surface complexes requires knowledge of both surface ion concentration and distribution of surface acidity sites, both free and occupied. Third, the potential distribution of EDL allows the estimate of electrostatic interaction energy between similar and dissimilar surfaces, which are essential to aggregation and hetero-aggregation, respectively, using the Derjaguin—Landau—Verwey—Overbeek (DLVO) theory (Li et al., 2019). The stability of NPs in freshwater depends on the energy barrier between repulsive electrostatic energy and attractive Van der Waals energy.

Conclusion

The accurate measurement of zeta potential of NPs is not a trivial task and should be conducted vigorously. The size of plastic particles affects not only the relevance of sedimentation but also the efficiency and pattern of light scattering. For NPs with size smaller than 100 nm, the accuracy of electrophoretic mobility measurement could be affected by Brownian motion because of the weak scattering efficiency and high diffusivity. The selection of correction function is crucial for the calculation of zeta potential using electrophoretic mobility data, especially when the size of NPs is comparable to the thickness of EDL. The optimization of the number concentration of the suspension is a prerequisite for the measurement of zeta potential to avoid the complication of EDL structure because of double layer overlapping and multiple scattering. For PS latex, the optimal number concentration was 10^{10}–10^{13} #/L. The effect of EDL compression at various ionic strengths on zeta potential of six synthesized NPs could be described by the Gouy–Chapman EDL model, enabling the estimation of surface potential and surface charge density. This information is invaluable for elucidating the surface acidity, stability, and adsorption process of NPs.

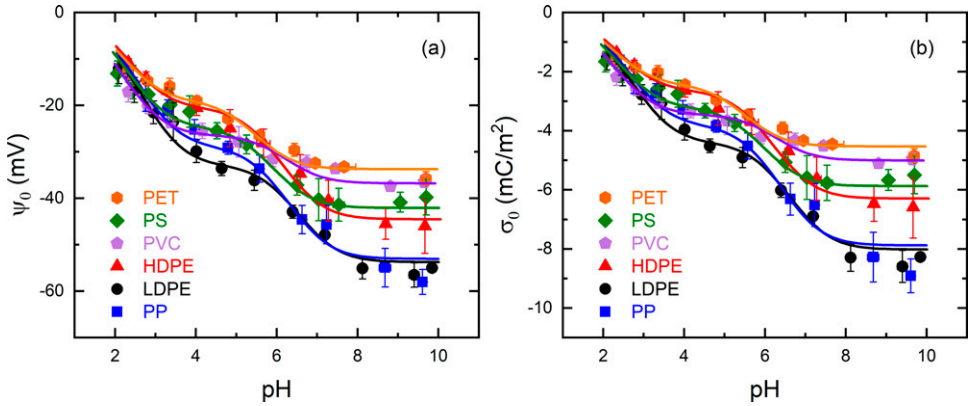

FIG. 7. **(a)** Surface potential and **(b)** surface charge density as a function of pH of six resynthesized NPs in 3×10^{-3} M $NaClO_4$.

Authors' Contributions

J.-Y.L.: Conceptualization, data curation, formal analysis, investigation, writing—original draft, and writing—reviewing and editing. I.L.: Resources and methodology. C.F.: Data curation and resources. H.K.: Funding acquisition and writing—reviewing and editing. C.-P.H.: Conceptualization, supervision, and writing—reviewing and editing.

Author Disclosure Statement

No competing financial interests exist.

Funding Information

This work is supported by the National Research Foundation of Korea in a grant funded by the Korea government (MSIT) (No. 2020R1A2C2101347) and the Graduate Program for Plastic-free Society funded by Korea Environmental Industry and Technology Institute. Additional support was provided by the Ministry of Science and Technology, Taiwan, to Jui-Yen Lin, under contract No. MOST-110–2917-I-564-033.

Supplementary Material

Supplementary Data S1

References

Ali I, Tan X, Xie Y, et al. Recent innovations in microplastics and nanoplastics removal by coagulation technique: Implementations, knowledge gaps and prospects. Water Res 2023; 245:120617; doi: 10.1016/j.watres.2023.120617

Alimi OS, Farner Budarz J, Hernandez LM, et al. Microplastics and nanoplastics in aquatic environments: Aggregation, deposition, and enhanced contaminant transport. Environ Sci Technol 2018;52(4):1704–1724; doi: 10.1021/acs.est.7b05559

Bayarkhuu B, Byun J. Optimization of coagulation and sedimentation conditions by turbidity measurement for nano- and microplastic removal. Chemosphere 2022;306:135572; doi: 10.1016/j.chemosphere.2022.135572

Behrens SH, Christl DI, Emmerzael R, et al. Charging and aggregation properties of carboxyl latex particles: Experiments versus DLVO theory. Langmuir 2000;16(6):2566–2575; doi: 10.1021/la991154z

Bhattacharjee S. DLS and Zeta Potential – What They Are and What They Are Not? J Control Release 2016;235:337–351.

Borkovec M, Behrens SH, Semmler M. Observation of the mobility maximum predicted by the standard electrokinetic model for highly charged amidine latex particles. Langmuir 2000;16(11):5209–5212; doi: 10.1021/la9916373

Caputo F, Vogel R, Savage J, et al. Measuring particle size distribution and mass concentration of nanoplastics and microplastics: Addressing some analytical challenges in the submicron size range. J Colloid Interface Sci 2021;588:401–417; doi: 10.1016/j.jcis.2020.12.039

Chassagne C, Ibanez M. Hydrodynamic size and electrophoretic mobility of latex nanospheres in monovalent and divalent electrolytes. Colloids Surf Physicochem Eng Asp 2014;440: 208–216; doi: 10.1016/j.colsurfa.2012.08.054

Enfrin M, Dumée LF, Lee J. Nano/Microplastics in Water and Wastewater Treatment Processes – Origin, Impact and Potential Solutions. Water Res 2019;161:621–638; doi: 10.1016/j.watres.2019.06.049

Fan R, Chen C, Lin J, et al. Adsorption characteristics of ammonium ion onto hydrous biochars in dilute aqueous solutions. Bioresour Technol 2019;272:465–472.

Feng C, Huang M, Huang C. Specific chemical adsorption of selected divalent heavy metal Ions onto Hydrous γ-Fe2O3-Biochar from Dilute Aqueous Solutions with pH as a Master Variable. Chem Eng J 2023;451:138921; doi: 10.1016/j.cej.2022.138921

Fu W, Min J, Jiang W, et al. Separation, Characterization and Identification of Microplastics and Nanoplastics in the Environment. Sci Total Environ 2020;721:137561; doi: 10.1016/j.scitotenv.2020.137561

Ganesan S, Ruendee T, Kimura SY, et al. Effect of biofilm formation on different types of plastic shopping bags: Structural and physicochemical properties. Environ Res 2022;206: 112542; doi: 10.1016/j.envres.2021.112542

Grigorescu RM, Grigore ME, Iancu L, et al. Waste electrical and electronic equipment: A review on the identification methods for polymeric materials. Recycling 2019;4(3):32; doi: 10.3390/recycling4030032

Hassan PA, Rana S, Verma G. Making sense of Brownian motion: Colloid characterization by dynamic light scattering. Langmuir 2015;31(1):3–12; doi: 10.1021/la501789z

Hunter RJ. Chapter 3 – The Calculation of Zeta Potential. In: Zeta Potential in Colloid Science. (Hunter RJ. Ed) Academic Press: Cambridge, Massachusetts; 1981; pp. 59–124.

Jabeen F, Chen M, Rasulev B, et al. Refractive indices of diverse data set of polymers: A computational QSPR based study. Comput Mater Sci 2017;137:215–224; doi: 10.1016/j.commatsci.2017.05.022

Karmakar S. Particle Size Distribution and Zeta Potential Based on Dynamic Light Scattering: Techniques to Characterise Stability and Surface Distribution of Charged Colloids. Studium Press: India; 2019; pp. 117–159.

Kim M-J, Herchenova Y, Chung J, et al. Thermodynamic Investigation of Nanoplastic Aggregation in Aquatic Environments. Water Res 2022;226:119286; doi: 10.1016/j.watres.2022.119286

Kobayashi M. Electrophoretic Mobility of Latex Spheres in the Presence of Divalent Ions: Experiments and Modeling. Colloid Polym Sci 2008;286(8–9):935–940; doi: 10.1007/s00396-008-1851-9

Kobayashi M. An Analysis on Electrophoretic Mobility of Hydrophobic Polystyrene Particles with Low Surface Charge Density: Effect of Hydrodynamic Slip. Colloid Polym Sci 2020;298(10):1313–1318; doi: 10.1007/s00396-020-04716-2

Lehner R, Weder C, Petri-Fink A, et al. Emergence of nanoplastic in the environment and possible impact on human health. Environ Sci Technol 2019;53(4):1748–1765; doi: 10.1021/acs.est.8b05512

Li Y, Wang X, Fu W, et al. Interactions between Nano/Micro plastics and suspended sediment in water: Implications on aggregation and settling. Water Res 2019;161:486–495; doi: 10.1016/j.watres.2019.06.018

Lin J-Y, Lee I, Tzeng J-H, et al. The surface acidity of freshly synthesized microplastics particles in simple electrolyte. Colloids Surf Physicochem Eng Asp 2023;675:132000; doi: 10.1016/j.colsurfa.2023.132000

Lins TF, O'Brien AM, Zargartalebi M, et al. Nanoplastic state and fate in aquatic environments: Multiscale modeling. Environ Sci Technol 2022;56(7):4017–4028; doi: 10.1021/acs.est.1c03922

Lu X, Zeng F, Wei S, et al. Effects of Humic Acid on Pb2+ Adsorption onto Polystyrene Microplastics from Spectroscopic

Analysis and Site Energy Distribution Analysis. Sci Rep 2022; 12(1):8932; doi: 10.1038/s41598-022-12776-3

Lunardi CN, Gomes AJ, Rocha FS, et al. Experimental methods in chemical engineering: Zeta potential. Can J Chem Eng 2021;99(3):627–639; doi: 10.1002/cjce.23914

Mätzler C. MATLAB Functions for Mie Scattering and Absorption, Version 2. IAP Res Rep 2002;8(1):9.

Mitrano DM, Wick P, Nowack B. Placing nanoplastics in the context of global plastic pollution. Nat Nanotechnol 2021; 16(5):491–500; doi: 10.1038/s41565-021-00888-2

Nguyen T-B, Ho T-B-C, Huang CP, et al. Adsorption of Lead (II) onto PE Microplastics as a Function of Particle Size: Influencing factors and adsorption mechanism. Chemosphere 2022;304:135276; doi: 10.1016/j.chemosphere.2022.135276

Nishiya M, Sugimoto T, Kobayashi M. Electrophoretic mobility of carboxyl latex particles in the mixed solution of 1:1 and 2:1 electrolytes or 1:1 and 3:1 electrolytes: Experiments and modeling. Colloids Surf Physicochem Eng Asp 2016;504: 219–227; doi: 10.1016/j.colsurfa.2016.05.045

Niskanen I, Forsberg V, Zakrisson D, et al. Determination of nanoparticle size using Rayleigh approximation and Mie theory. Chem Eng Sci 2019;201:222–229; doi: 10.1016/j.ces .2019.02.020

O'Brien RW, White LR. electrophoretic mobility of a spherical colloidal particle. J Chem Soc, Faraday Trans 2 1978;74(0): 1607–1626.

Ohshima H. Approximate analytic expression for the electrophoretic mobility of a spherical colloidal particle. J Colloid Interface Sci 2001;239(2):587–590; doi: 10.1006/jcis.2001.7608

Pei H, Zhang S. Molecular dynamics study on the zeta potential and shear plane of montmorillonite in NaCl solutions. Appl Clay Sci 2021;212:106212; doi: 10.1016/j.clay.2021.106212

Scarlett B. (ed). Electrophoretic Light Scattering. In: Particle Characterization: Light Scattering Methods. Particle Technology Series Kluwer Academic Publishers: Dordrecht; 2002; pp. 289–343; doi: 10.1007/0-306-47124-8_6

Tantra R, Schulze P, Quincey P. Effect of nanoparticle concentration on Zeta-Potential measurement results and reproducibility. Particuology 2010;8(3):279–285; doi: 10.1016/j.partic.2010.01.003

Thomas TE, Aani SA, Oatley-Radcliffe DL, et al. Laser doppler electrophoresis and electro-osmotic flow mapping: A novel methodology for the determination of membrane surface zeta potential. J Membr Sci 2017;523:524–532; doi: 10.1016/j .memsci.2016.10.029

Weng C-H, Huang CP, Allen HE, et al. Cr (VI) Adsorption onto hydrous concrete particles from groundwater. J Environ Eng 2001;127(12):1124–1131; doi: 10.1061/(ASCE)0733-9372(2001)127:12(1124

Yu X, Ladewig S, Bao S, et al. Occurrence and distribution of microplastics at selected coastal sites along the Southeastern United States. Sci Total Environ 2018;613-614:298–305; doi: 10.1016/j.scitotenv.2017.09.100